Anomalous anisotropy of re-entrant $Ni_{77}Mn_{23}$ film

1997 J. Phys.: Condens. Matter 9 6433

(http://iopscience.iop.org/0953-8984/9/30/012)

J. Phys.: Condens. Matter **9** (1997) 6433–6445. Printed in the UK PII: S0953-8984(97)81495-6

Anomalous anisotropy of re-entrant $Ni_{77}Mn_{23}$ film

Mustafa Özdemir†, Bekir Aktaş‡, Yıldırhan Öner§, T Sato‖ and T Ando‖

† Department of Physics, Marmara University, Göztepe-Istanbul, Turkey
‡ Department of Physics, Gebze Institute of Technology, Gebze-Kocaeli, Turkey
§ Department of Physics, Istanbul Technical University, Maslak-Istanbul, Turkey
‖ Department of Instrumentation Engineering, Faculty of Science and Technology, Keio University, Japan

Received 3 February 1997, in final form 29 April 1997

Abstract. Re-entrant polycrystalline $Ni_{77}Mn_{23}$ films, 600 Å thick, grown on a quartz substrate by using an electron beam evaporation technique, have been investigated. A spin-wave resonance (SWR) technique has been used to study the magnetic properties of the films. The SWR spectra exhibit highly anisotropic behaviour with respect to the film normal. When the sample is rotated around the film normal in a fixed applied field, both the resonance fields and the line-shapes are changed. This unexpected behaviour—for a polycrystalline film—has been attributed to a growth-induced geometric (oblique) anisotropy. The SWR spectra have been successfully analysed by using this oblique anisotropy term in addition to usual magnetocrystalline effective bulk, surface, and unidirectional anisotropy terms in the magnetic free energy. A substantial and temperature-dependent growth-induced geometric anisotropy has been obtained, beside the usual bulk and surface anisotropies. A strong correlation between the surface and oblique anisotropy has been found. This correlation has been attributed to a manifestation of the influence of easy-plane surface anisotropy along the fibre axes of individual grains on the effective magnetic anisotropy energy.

1. Introduction

NiMn alloys have been intensively investigated, either in bulk or in thin-film forms, mainly because of their unusual magnetic behaviour—such as the displaced hysteresis loop obtained upon cooling the sample in an external field, and a maximum in the ac susceptibility [1–9]. The system shows a variety of magnetic anisotropies [7–11], and does not easily reach the magnetic configuration having energy minima. Most of these properties are greatly affected by the thermal history of the sample. As is well known, the temperature annealing (or quenching) treatment of NiMn alloys strongly affects the magnetic parameters, such as the exchange anisotropy energy [4, 5]. This implies that the system has porous structure when it is quenched down to room temperature from high temperatures. In other words the atoms are not mobile enough to approach their minimum-energy configuration at room temperature. These properties make the NiMn system a good candidate as regards producing a growth-induced microscopic geometric anisotropy in the thin-film form.

The geometric anisotropy was observed first by Knorr and Hoffman [12], for vacuum-deposited thin iron films. They reported that a fibre axis structure was induced during the evaporation, and that this fibre axis tilts in a similar direction of incidence to that of the metallic flux, varied from the normal to the substrate. As the fibre axis was no longer normal to the plane of the film, so-called geometric anisotropy was induced, depending on the geometric location of the evaporating filament.

0953-8984/97/306433+13$19.50

For the determination of the magnetic anisotropies of thin films, the ferromagnetic resonance (FMR) technique (or spin-wave resonance (SWR) technique) is ideal [13]. The anisotropy parameters are derived from the resonance-field values, which do not depend on the real volume of the specimen, whereas the torque and magnetization techniques do. Also, SWR forms the basis of one of the most sensitive techniques for getting a signal from a very tiny sample. In this study, we observed a growth-induced geometric (oblique) anisotropy for thin films of the $Ni_{77}Mn_{23}$ alloy by the SWR technique. The experimental results were successfully interpreted by introducing a geometric anisotropy, and a satisfactory agreement has been found between the experimental data and the theory.

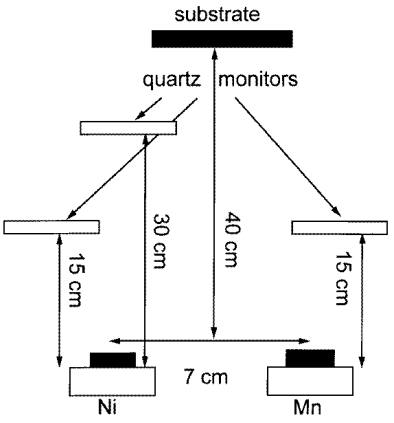

Figure 1. A simple sketch of the evaporation set-up used to deposit $Ni_{77}Mn_{23}$ thin films.

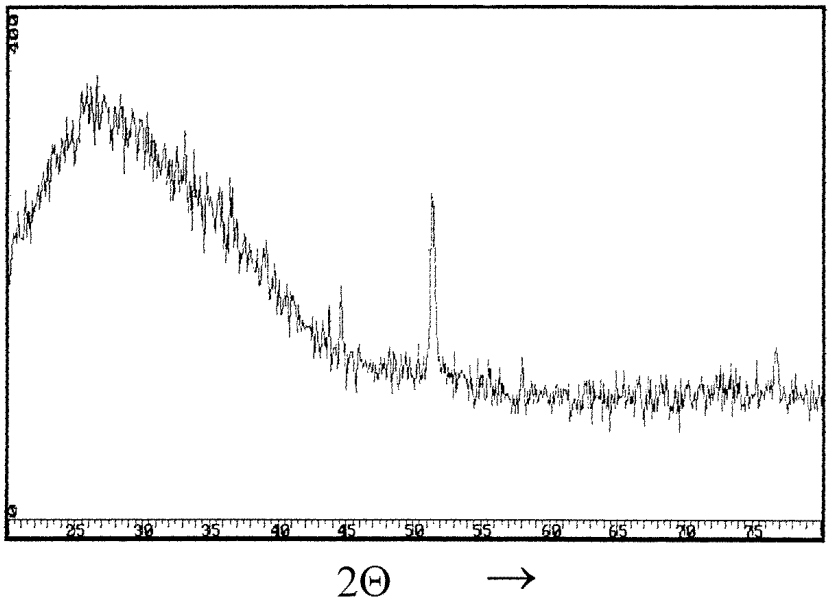

Figure 2. The x-ray diffraction spectra of $Ni_{77}Mn_{23}$.

2. Experimental results

The electron beam technique has been used to grow thin films of $Ni_{77}Mn_{23}$ alloy by co-evaporation of the constituents. The evaporation set-up is sketched in figure 1. The base pressure was 5×10^{-8} Torr. Carefully cleaned quartz was used as a substrate. The errors in the Mn concentration and the film thickness are less than 0.5% and 5% respectively. The x-ray diffraction data in figure 2 indicate a polycrystalline structure.

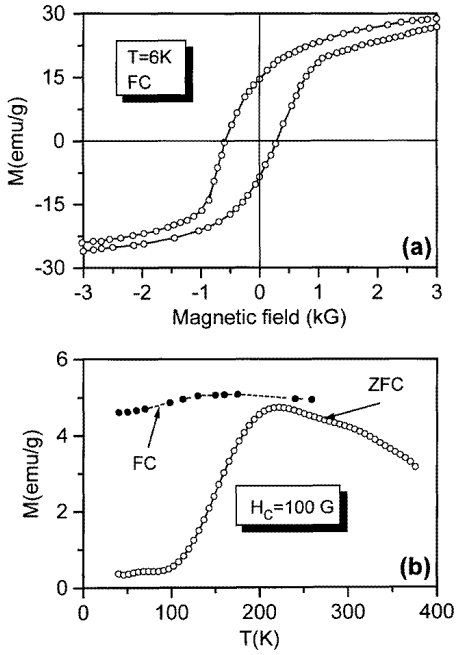

Figure 3. (a) A magnetic hysteresis loop recorded after cooling the sample down to 6 K in an external field in the film plane; (b) DC magnetization data as a function of temperature for zero-field-cooling (ZFC) and field-cooling (FC) cases in an external field of 100 Oe.

A SQUID was used to carry out the DC magnetization measurements as a function of temperature. The data were taken after cooling the sample in an external DC field of 100 Oe in the sample plane (the FC case) or in zero field (the ZFC case). As can be seen from figure 3, the hysteresis loop at 6 K for the FC case is considerably wider, and is shifted to a negative field of about 100 G. The values of the magnetization for the FC and ZFC cases are slightly different from each other. This difference is maintained even up to room temperatures. The field treatments considerably affect the measured values. All of the above results indicate spin-glass properties for $Ni_{77}Mn_{23}$ film.

Ferromagnetic resonance (FMR or SWR) measurements have been carried out by using a Commercial Varian E line spectrometer operating at X-band (the microwave frequency is about 9.4 GHz). The experimental axis system and the sample geometry are illustrated in figure 4.

Figure 5 displays room temperature SWR spectra taken at some selected orientations of the external field with respect to the coordinate system in figure 4. A magnetic field was applied in two different planes, which are perpendicular to each other and to the film plane. The angle, θ_H, of the applied field is measured from the film normal in both planes. The

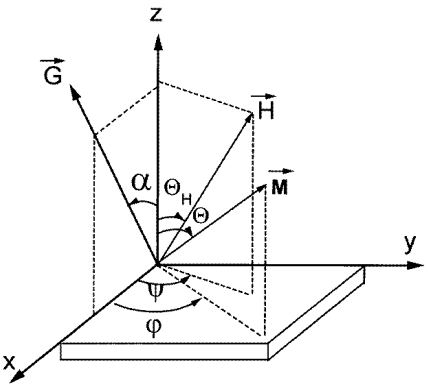

Figure 4. The relative orientations of the magnetization $\boldsymbol{M}$, external magnetic field $\boldsymbol{H}$, oblique anisotropy axis $\boldsymbol{G}$, and xyz-axes system with respect to the film.

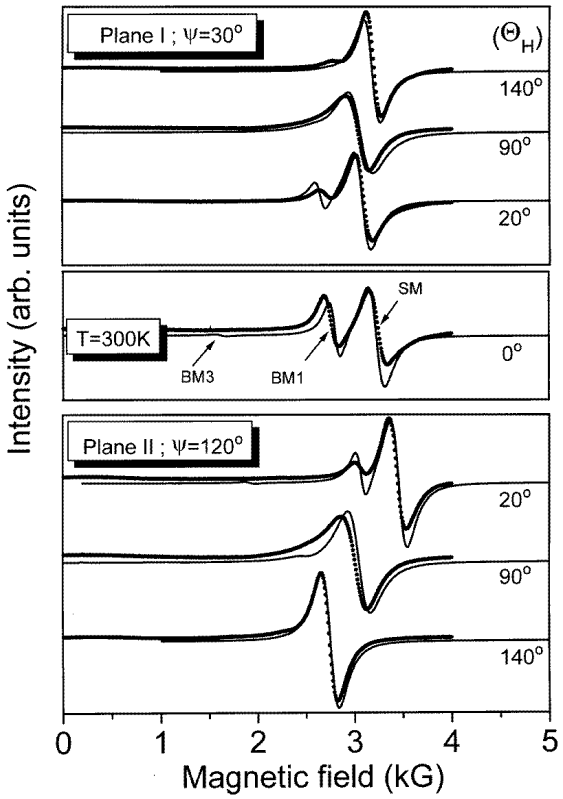

Figure 5. Spin-wave resonance spectra in both planes (see the text) for different orientations of the applied magnetic field at $T = 300$ K. The points show the measured spectra. The best fits are given by solid lines. BMi and SM represent the bulk and the surface modes respectively for perpendicular geometry ($\theta_H = 0$).

spectra comprise two main modes having comparable intensities when the deviation of the external field from the film normal is small enough. As the external field is rotated away

from the film normal, the relative amplitude of the mode at the highest field rises, and the separation of these two modes progressively decreases with increasing polar angle, θ_H, and they overlap when the angle θ_H takes a value of around 45° in both planes. When this angle increases to larger values, only a single absorption mode is observed. These are some examples of characteristic behaviour of a classical spin-wave resonance spectrum having a surface mode with a uniaxial easy-plane surface anisotropy field.

However, the polar angle dependence of the resonance-field values, the line-shapes, and the line amplitudes for plane I (where the azimuth angles $\phi = \psi = 120°$; hereafter PI) are quite different to those for plane II (where $\phi = \psi = 30°$; hereafter PII). The spectra are not symmetrical with respect to the film plane even in the same plane. In particular, the resonance-field values are not equal for the same values of the polar angle. PII is much more anisotropic than PI. Naturally, for any homogeneous polycrystalline magnetic film, these two planes are anticipated to be equivalent to each other, and no difference between the spectra for PI and PII would be expected. These asymmetric behaviours of the SWR spectra (the ϕ, ψ-dependence, and the asymmetry with respect to the film plane) imply the existence of an anomalous anisotropy in the polycrystalline NiMn film.

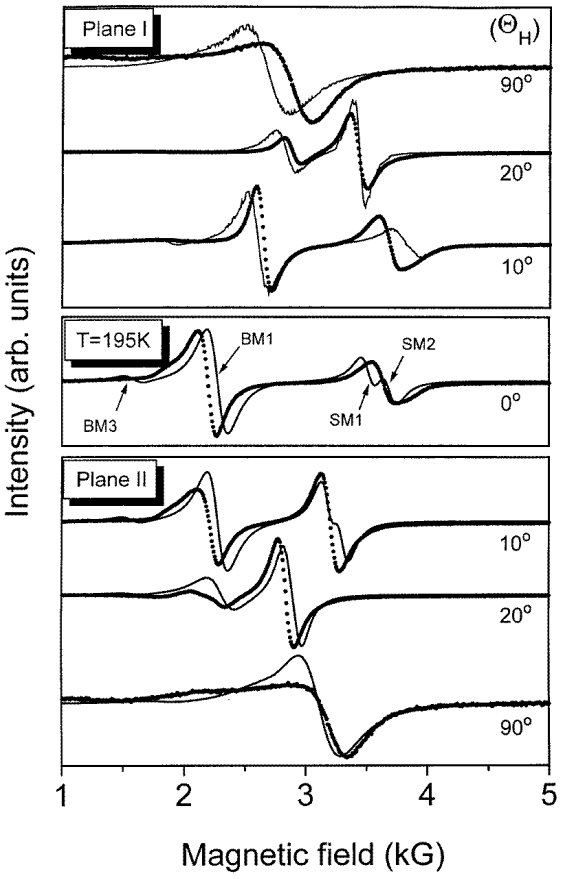

Figure 6. Spin-wave resonance spectra in both planes for different orientations of the applied magnetic field at $T = 195$ K. The points show the measured spectra. The best fits are given by solid lines.

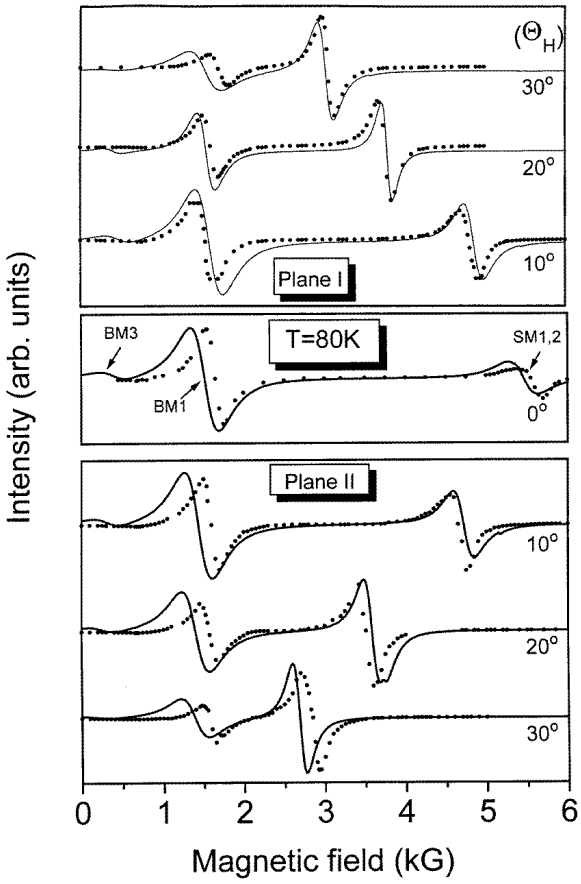

Figure 7. Spin-wave resonance spectra in both planes for different orientations of the applied magnetic field at $T = 80$ K. The points show the measured spectra. The best fits are given by solid lines. As can be seen, the separation of the surface mode from the bulk modes considerably increases as the temperature decreases.

These asymmetric angular dependencies have also been observed at lower temperatures, as shown in figures 6 and 7. Moreover, for perpendicular geometry ($\theta_H = 0$), the spectra at lower temperature are quite different to those at room temperature. The separation of the major peaks from each other increases with decreasing temperature, while the spectrum shifts to lower fields as a whole. For a pure ferromagnetic film, the spectrum at $\theta_H = 0$ is expected to shift to higher fields due to the demagnetizing field, which rises with increasing magnetization at lower temperatures. However, it should be noted that the NiMn alloys at this composition rate are re-entrant, and show spin-glass properties. Therefore, at lower temperature, exchange anisotropy (unidirectional anisotropy) is induced, so as to keep the exchange-field direction always independent of the crystalline axes. If the relaxation of the anisotropy is quick enough, this field manifests itself along the instantaneous magnetization direction. Thus, this exchange field is added to the effective field, and results in a decrease in the contribution of the external field for the resonance-field values. That is, the exchange anisotropy, $\boldsymbol{H}_{exc}$, accounts for the shift both of the hysteresis loop and the SWR spectrum to lower field. Also the peak at the highest field at low temperatures is

split, and the relative amplitudes of the two resulting peaks progressively decrease with decreasing temperature for perpendicular geometry (when the field is applied along the film normal). This behaviour clearly indicates that these two peaks belong to the surface modes. The surface anisotropy fields for the two surfaces are very close to each other, and they increase at low temperatures.

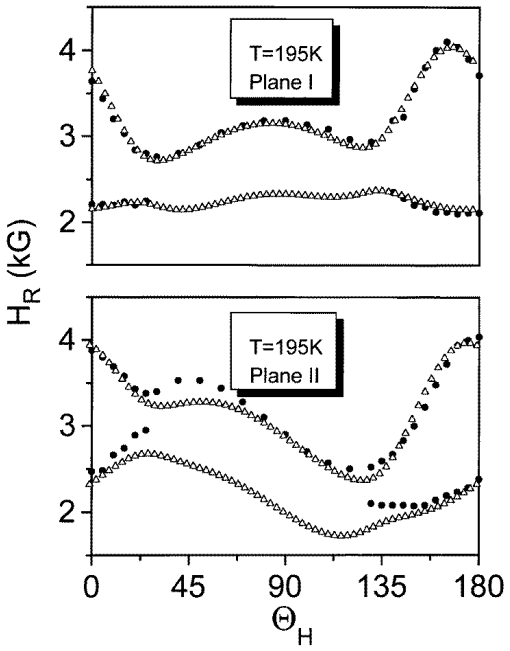

Figure 8. The resonance-field values in both the isotropic and the anisotropic planes, as functions of the applied magnetic field at 195 K. The points show the resonance-field values obtained from the experimental SWR spectra. The best fits are indicated by △.

The angular variations of the resonance fields of the two most intense peaks in both planes (PI and PII) are plotted in figure 8 for a temperature of 195 K. As can be seen from this figure, plane PII seems to be more anisotropic than plane PI as regards the resonance-field values. The curves for the two planes are not symmetric with respect to the film normal. These anisotropies are also temperature dependent. These temperature dependences are seen more clearly in figure 9. The low-temperature angular variation of the resonance field is much sharper than that at room temperature. These differences partly arise from the demagnetizing field, which increases with the magnetization at lower temperature, and partly from the temperature dependence of the geometric anisotropy. As stated earlier, for a polycrystalline ferromagnetic film only a uniaxial anisotropy energy having the film normal as a symmetry axis can be expected. The angular curves of the resonance fields at lower temperature are more symmetrical with respect to the 90° angle than the curve at higher temperature, as seen in figures 8 and 9. Therefore the major contribution to this anisotropy at low temperatures should be shape anisotropy (originating from the demagnetizing field), in addition to any perpendicular anisotropy (arising from magnetostriction or any other causes). The asymmetric behaviour with respect to the film normal should arise from some growth-induced anisotropy, as will be explained below.

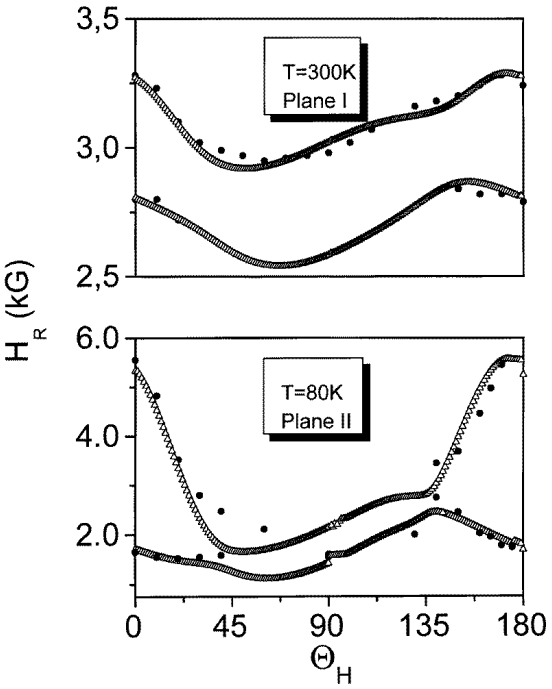

Figure 9. The resonance-field values as a function of the applied magnetic field at 300 K (PI) and 80 K (PII). The full circles show the resonance-field values obtained from the experimental SWR spectra. The best fits are indicated by △.

3. The theoretical model

In order to explain these peculiar behaviours, we used a growth-induced geometric (oblique) anisotropy term, in addition to the usual effective uniaxial and unidirectional (exchange) bulk and surface anisotropy energies for re-entrant NiMn films. The free energies for the system is

$$E = E_Z + E_b + E_g + E_s$$

where

$$E_Z = -\boldsymbol{M} \cdot (\boldsymbol{H} + \boldsymbol{H}_{exc})[\cos(\theta)\cos(\theta_H) + \sin(\theta)\sin(\theta_H)\cos(\varphi - \psi)] \quad (1a)$$

$$E_b = K_{eff}\sin^2(\theta) \quad (1b)$$

where $\boldsymbol{M}$ is the magnetization, and $\boldsymbol{H}_{exc}$ is the field-induced exchange anisotropy for the re-entrant NiMn system. The exchange anisotropy (or field-induced unidirectional anisotropy) is a common property of spin glasses and re-entrant systems, and NiMn alloys are known to exhibit spin-glass and re-entrant properties, depending on the concentration of Mn. The composition rate of $Ni_{77}Mn_{23}$ alloy corresponds to the critical point between the re-entrant and pure spin-glass regimes. Therefore our film should exhibit exchange anisotropy. This anisotropy can relax over time. If the relaxation time is longer than the DC measurement time, it is rigidly linked to the lattice, and manifests itself in the shift of both the hysteresis loop and the resonance field at very low temperatures. In fact, this anisotropy can rotate elastically or dissipatively, as shown in the literature [1, 16]. This rotation results in a broadening of both the hysteresis loop and the resonance curve.

In equation (1), θ_H and ψ are the spherical angles of the applied field, while θ and φ are the usual spherical polar angles for $\boldsymbol{M}$. In equation (1), K_{eff} $(=K_1-2\pi M^2)$ represents the effective uniaxial anisotropy parameter, including both the shape anisotropy, $2\pi M^2$ (the demagnetizing energy), and any kind of stress-induced and growth-induced perpendicular uniaxial anisotropy K_1. The third term in equation (1) represents the growth-induced oblique anisotropy, which is roughly assumed to be, as in [13],

$$E_g(\theta,\varphi,\alpha) = K_g\left\{\sin^2\theta|\cos(2\alpha)+\sin^2(\alpha)\sin^2\varphi)| - \frac{1}{2}\sin(2\theta)\sin(2\alpha)\cos(\varphi)\right\} \tag{2}$$

where K_g is the geometric anisotropy parameter, and α the angle of the fibre axis (in the xz-plane) with respect to the film normal, as shown in figure 4. The fourth term in equation (1) accounts for the surface anisotropy energy. Here, the z-axis is chosen to lie along the film normal, and the microwave component of the applied field is chosen to be parallel to x-axis in the film plane. For a general direction of the static magnetic field, $\boldsymbol{H}$, the basic dispersion relation for the spin wave is given [13, 14, 17] as

$$\left(\frac{\omega}{\gamma}\right)^2 = \left(\frac{1}{M\sin^2\theta}\frac{\partial^2 E}{\partial\varphi^2}+Dk_n^2\right)\left(\frac{1}{M}\frac{\partial^2 E}{\partial\theta^2}+Dk_n^2\right) - \left(\frac{1}{M\sin\theta}\frac{\partial^2 E}{\partial\varphi\,\partial\theta}\right)^2 + \frac{1}{\gamma^2T_2^2} \tag{3}$$

where γ is the gyromagnetic ratio, ω is the microwave frequency, D is the exchange stiffness parameter, and k_n is the spin-wave vector for the nth mode. In equation (3), T_2 is the relaxation time of the dynamic component of the magnetization, and determines the linewidth of the peaks in the SWR spectra $(1/T_2=\gamma\,\Delta H)$. Here θ and φ are determined by the static equilibrium conditions

$$\frac{\partial E}{\partial\varphi} = \boldsymbol{M}\cdot(\boldsymbol{H}+\boldsymbol{H}_{exc})\sin(\theta)\sin(\theta_H)\sin(\varphi-\psi) + K_g\left\{\sin(2\varphi)\sin^2(\alpha)\sin^2(\theta)-\frac{1}{2}\sin(2\theta)\sin(2\alpha)\sin(\varphi)\right\}=0 \tag{4a}$$

$$\frac{\partial E}{\partial\theta} = K_{eff}\sin(2\theta)+\boldsymbol{M}\cdot(\boldsymbol{H}+\boldsymbol{H}_{exc})[\sin(\theta)\cos(\theta_H)-\cos(\theta)\sin(\theta_H)\cos(\varphi-\psi)] + K_g\{\sin(2\theta)[\cos(2\alpha)+\sin^2(\alpha)\sin^2(\varphi)]-\cos(2\theta)\sin(2\alpha)\cos(\varphi)\}=0 \tag{4b}$$

for the magnetization. Thus, using equations (1) and (3) in the general resonance condition (equation (2)), one can obtain the following expression for the resonance field for the nth SWR mode:

$$\left(\frac{\omega}{\gamma}\right)^2 = AB - C^2 + \frac{1}{\gamma^2T_2^2} \tag{5}$$

where

$$A = (H+H_{exc})[\cos(\theta)\cos(\theta_H)+\sin(\theta)\sin(\theta_H)\cos(\varphi-\psi)] + 2\frac{K_{eff}}{M}\cos(2\theta) + 2\frac{K_g}{M}[\cos(2\theta)|\cos(2\alpha)+\sin^2(\alpha)\sin^2(\varphi)|+\sin(2\theta)\sin(2\alpha)\cos(\varphi)] + Dk_n^2$$

$$B = (H+H_{exc})[\cos(\theta)\cos(\theta_H)+\sin(\theta)\sin(\theta_H)\cos(\varphi-\psi)] + 2\frac{K_{eff}}{M}\cos^2(\theta) + 2\frac{K_g}{M}[\cos^2(\theta)|\cos(2\alpha)+\sin^2(\alpha)\sin^2(\varphi)| + \frac{1}{2}\sin(2\theta)\sin(2\alpha)\cos(\varphi)+\sin^2(\alpha)\cos(2\varphi)] + Dk_n^2$$

$$C = (H + H_{exc})[\cos(\theta)\cos(\theta_H) + \sin(\theta)\sin(\theta_H)\cos(\varphi - \psi)] + 2\frac{K_g}{M}[\cos(\theta)\sin^2(\alpha)\sin(2\varphi) + \sin(\theta)\sin(2\alpha)\sin(\varphi)]$$

for a general direction of the measurement field after cooling the sample in the field along the film normal. The spin-wave vectors, k_n, are determined from the expressions [15]

$$\tan(k_n L) = \frac{k_n(P_1 + P_2)}{k_n^2 - P_1 P_2} \tag{6}$$

for the bulk modes, and from

$$\tanh(k_n L) = -\frac{k_n(P_1 + P_2)}{k_n^2 + P_1 P_2} \tag{7}$$

for the surface modes, where L is the film thickness, and P_i is the surface pinning parameter which is obtained from the axial surface anisotropy energy at the ith surface as follows [14, 15]:

$$P_i = (K_{si} L/D M_s)\cos(2\theta) + (\partial_n M_s)/M_s. \tag{8}$$

Here L is the film thickness, and K_{si} is the uniaxial surface anisotropy parameter:

$$E_s = K_s \cos^2\theta \tag{9}$$

for the ith surface. The second term in equation (8) comes from the inhomogeneous saturation magnetization at the surface of the film.

4. Discussion

We have calculated the theoretical spectra by using the above model. As one can see, the calculation of the theoretical spectra is very problematic. For a given parameter set and external-field orientation, first, the equilibrium angle, θ, is obtained by a computer procedure from the solution of equation (4). Secondly, using this value for θ in equation (8), the surface pinning parameter, P, is calculated. Thirdly, the spin-wave vectors, k'^s, for both the bulk and the surface modes, are obtained from the computer solution of equations (6) and (7) respectively, up to any desired mode number. Finally, these wave vectors for each of the spin-wave modes are used in the dispersion relation, equation (5), to get the resonance frequency. The same values are also used in the very high-frequency (microwave) ac susceptibility expression (equation (26b) in reference [15]), which corresponds to the observed SWR spectra. It should be noted that in any conventional ESR spectrometer, the external field is scanned while the frequency remains fixed. Therefore, all of the above procedures should be followed for a certain external field. Most of the expressions include various trigonometric functions, and have many singularities and multiple roots for the parameters to be solved for. In particular, in the calculation of the resonance-field values for any mode, starting with a selected value for H, all of the above work must be repeated iteratively to achieve the desired accuracy for H.

The theoretical results are given in figures 5, 6, 7, 8, and 9, with the corresponding experimental ones. The parameters used in the calculations are given in table 1. The model seems to explain the experimental data quite well. Satisfactory agreements have been found between the theoretical and the experimental spectra for almost all temperatures, and for any direction of the external magnetic field. It should be emphasized that almost exact agreement is obtained if one uses an independent fitting for each spectrum, but in order to be consistent we have in fact used the same parameter set for the spectra for all directions at a

Table 1. Fitting parameters.

T (K)	$2K_{eff}/M_s$ (kG)	$2K_g/M_s$ (kG)	ΔH_{p-p}(bulk) (G)	$K_{s1}L/DM_s$	$K_{s2}L/DM_s$	D (10^{-10} G cm^2)	H_{exc} (kG)
300	-0.06 ± 0.05	0.80 ± 0.05	120 ± 10	-4.5 ± 0.5	-4.5 ± 0.5	3.5 ± 0.2	0.00 ± 0.05
195	-1.00 ± 0.05	1.70 ± 0.05	110 ± 10	-11 ± 0.5	-12 ± 0.5	5.0 ± 0.2	0.15 ± 0.05
80	-2.00 ± 0.05	3.00 ± 0.05	140 ± 10	-18.2 ± 0.5	-18 ± 0.5	4.0 ± 0.2	0.55 ± 0.05

certain temperature. Some small discrepancies between the theoretical and the experimental data for some orientations of the external field can be attributed partly to the experimental errors in the measured angles, and partly to the proposed model for the geometric and usual axial anisotropy energy contribution, in which the higher-order terms were neglected. Nevertheless, a model having this form seems to be acceptable.

As seen from table 1, the magnetic parameters change with the temperature. The effective bulk anisotropy parameter, K_{eff}, increases with decreasing temperature. The demagnetizing field, $-4\pi M$, is the dominant contribution to the effective anisotropy energy parameter, which reaches values of about 2000 G. Using this effective anisotropy energy, and refining $4\pi M$ (the magnetization in figure 3) from it, one can obtain an easy-axis (film-normal) crystalline anisotropy. This easy-axis anisotropy can be seen from the hysteresis loop in figure 3, as well. As can be seen in this figure, the magnetization measured in the film plane for the FC case is not saturated even in a field of 1 kOe. On the other hand, the hysteresis curve measured for a perpendicular field is very sharp (we have not shown this in the figure). That is, the film plane is a hard direction, and the film normal is an easy direction for the spins, which is in agreement with the results from the SWR data. The hysteresis loop for the field-cooling case is shifted to lower fields. This shift was attributed to unidirectional anisotropy due to competing interactions between antiferromagnetic Mn–Mn and ferromagnetic Ni–Ni, Ni–Mn pairs, as reported for bulk samples in the literature [1–3]. As the temperature rises, the magnetization, and therefore also the effective anisotropy parameter are decreased. No strong temperature dependence for the crystalline bulk anisotropy energy is expected.

A strong correlation is seen between the magnetization and the geometric anisotropy parameters in table 1. As a matter of fact, this correlation implies similar physical origins for both of the anisotropy energies. As explained above, the dominant term in the effective bulk anisotropy energy is the demagnetizing field which arises from the macroscopic shape of the film, while the proposed geometric (oblique) anisotropy energy originates from the shapes of the local microscopic grains formed during the deposition of the films. Each grain has its own demagnetizing field, due to its saturation magnetization.

The possible formation of granular structure can be understood from figure 1. The beam directions from Ni and Mn sources are in the plane of the paper, and they are not perpendicular to the film plane. It can be expected that, at the early stage of growth, each incident beam will tend to tilt the grains of the NiMn alloy in the film along its own direction. Since the atomic percentage of Ni is much higher than that of Mn, the resultant granular structure may be grown along the Ni beam direction. In addition to this, the Ni and Mn beams tend to deposit on different sides of the grains—that is, the side facing Ni may be Ni rich, while the other side, facing the Mn beam, is Mn rich, compared to the nominal value of 23% at the Mn sites in the alloy. Therefore, it is quite possible that the concentration in the granular structure varies from the Mn to the Ni side in the plane of the paper. This may be assumed as an additional effect that gives special

directions for the spins in the film plane. It should be noted that the angle characterizing the geometric anisotropy is between 10° and 20° from the film normal. This value is slightly larger than the angle of the beam from the film normal. The excess in the fitted value for α (which characterizes the geometric anisotropy axis) as compared to the beam angle can be accounted for by the inhomogeneity of the concentration in the granular structure.

The correlation between this anomalous anisotropy and the demagnetizing field is consistent with our geometric anisotropy interpretation. However, the exact origin of this anisotropy is not clear at present, and it is worth investigating in more detail. In fact, we are planning to do detailed research on this in the future. But in this paper, we would just like to give the first observations on the NiMn system, in which this anisotropy is quite large.

The exchange interaction parameter, D, shows a weak temperature dependence. The absolute values of this parameter fall in the range given in the literature [2, 15]. It starts to increase as the temperature decreases in the ferromagnetic regime, and passes through a maximum at around 120 K, which corresponds to the canting temperature, T_f, and then decreases again in the spin-glass regime below T_f. The exchange anisotropy field is induced at lower temperature, and its magnitude is larger than that for bulk samples [9]. Similar observations have been made in the literature [8, 9]. Other authors used bulk and thin films of the same $Ni_{76}Mn_{24}$ sample, and established that the thin-film sample has a much larger anisotropy than the bulk sample. It seems to be plausible to achieve this kind of temperature dependence for the exchange anisotropy energy.

As can be seen from columns 5 and 6 in table 1, the parameters for both of the surface anisotropy energies are almost the same. Unlike the magnetocrystalline anisotropy energy, the surface anisotropy parameters are strongly temperature dependent. The values of these parameters at 80 K are almost four times stronger than those at room temperature. So strong a temperature dependence is not expected for any magnetocrystalline surface anisotropy energy. The main contribution to the surface parameters should come from the exchange anisotropy interaction. The similar temperature behaviour of the unidirectional exchange anisotropy field supports this interpretation. Also, the increase in the geometric anisotropy at low temperature can be partly attributed to this exchange anisotropy induced on the surface of each individual grain.

In conclusion, the growth as a function of temperature of thin films of $Ni_{77}Mn_{23}$ alloy by an electron beam technique has been studied. Evidence for polycrystalline structure has been obtained from the x-ray diffraction data. The magnetization data showed this sample to have spin-glass properties. The anomalous magnetic anisotropy for polycrystalline film has been explained by using a geometric anisotropy originating from the local granular growth along the evaporated beam direction, which is the symmetry axis (fibre axis) of the grains. At very lower temperatures, the exchange anisotropy dominates over all other terms in the magnetic anisotropy energy. However, at intermediate temperatures, spin-wave resonance data can be explained well using the model mentioned above. The magnetic anisotropy parameters have been deduced from ESR data by adding an oblique anisotropy energy term into the usual magnetic energy in the same calculation procedure as is described in the literature.

Acknowledgment

This work was supported by TUBITAK, under Project No TBAG-1365.

References

[1] Öner Y and Aktaş B 1990 *Phys. Rev.* B **42** 2425
Aktaş B, Öner Y and Harris E A 1989 *Phys. Rev.* B **39** 528
[2] Abdul-Razzaq W and Kouvel J S 1984 *J. Appl. Phys.* **55** 1623
[3] Senoussi S 1983 *Phys. Rev. Lett.* **51** 2218
[4] Aitken R G, Cheung J D and Kouvel J S 1984 *J. Magn. Magn. Mater.* **30** L1
[5] Senoussi S 1985 *Phys. Rev.* B **31** 6086
[6] Abdul-Razzaq W and Wu M 1990 *35th Ann. Conf. on Magnetism and Magnetic Materials (San Diego, CA, 1990)* p 29
[7] Ando T, Sato T and Ohta E 1992 *J. Magn. Magn. Mater.* **113** 115
[8] Aktaş B, Öner Y and Durusoy H Z 1993 *J. Magn. Magn. Mater.* **119** 339
[9] Aktaş B and Öner Y 1993 *J. Phys.: Condens. Matter* **5** 5443
[10] Aktaş B 1993 *Solid State Commun.* **87** 1067
[11] Özdemir M, Aktaş B, Öner Y, Sato T and Ando T 1996 *J. Magn. Magn. Mater.* **164** 53
[12] Knorr T G and Hoffman R W 1959 *Phys. Rev.* **113** 4
[13] Kohmoto O and Alexander C Jr 1992 *J. Magn. Magn. Mater.* **116** 405
[14] Maksymowicz L J and Sendorek D 1983 *J. Magn. Magn. Mater.* **37** 177
[15] Aktaş B and Özdemir M 1994 *Physica* B **193** 125
[16] Abdul-Razzaq W and Kouvel J S 1986 *Phys. Rev.* B **35** 1764
[17] Wigen P E 1984 *Thin Solid Films* **114** 135